

Linking surface roughness with vertical coherent structures in the marine boundary layer near the Agulhas current

Hugo Jacquet¹, Alex Ayet², Fleur Couvreux³

¹Université Grenoble Alpes, CNRS, IGE, France

²CNRS, Université Grenoble Alpes, Inria, Grenoble INP, GIPSA-Lab, Grenoble, France.

³Université de Toulouse, Météo-France, CNRS, CNRM, France

Corresponding author: Hugo Jacquet, hugo.jacquet.work@gmail.com

Abstract

To be done

Plain Language Summary

To be done

1 Introduction

Vocabulary:

MABL = Marine Atmospheric Boundary Layer

Coherent structure = object detected by (Couvreux et al., 2010) that maximize the contribution of objects to the turbulent fluxes ($\langle uw \rangle$ and $\langle w\theta_v \rangle$)

Work hypothesis :

- Coherent structure of the MABL can be seen on SAR surface data.
- Coherent structure of the MABL can be detected with a conditional sampling based on passive tracer emission.

The main goal of this study is to answer the following questions:

- What is the internal structure of the MABL above a realistic SST front and how is it influenced by environmental conditions ?
- Can surface roughness retrieved from SAR satellite give information about the vertical structure of the MABL ?

2 The LES simulations

2.1 General considerations

Modeling a flow over an heterogeneity is a challenge (Fogarty et al., 2024). To address this, we design the experiment illustrated on Figure 1. We use the nesting capabilities of MesoNH (Lac et al., 2018, version 5.7.0) : two simulations are run in the same experiment. A first domain with low resolution is set up and we will call this domain the ‘dad’ domain. Lateral boundary conditions are cyclic in the West/East direction, and open in the North/South direction. This domain serves as a turbulence generator that will be injected in the second domain (the ‘son’ domain). The exchange of information is one way, meaning that the son is influenced by the dad but not the other way. The hope in such design is that the inflow characteristics will be improved compared to a son-only equivalent simulation with double open boundary conditions and with a shorter distance for the turbulence to develop. The validation of the inflow will be detailed in the section 2.2. Another way to have a turbulent inflow is the ‘turbulence recycling’ method described by Nagel et al. (2022) but it has only been tested in neutral conditions and we focus here on a heterogeneous SST gradient (in both X and Y directions) and so this second method would have required more testing before use.

We now describe the general configurations of the simulations. Two set of simulations have been produced: a turbulent inflow validation set (described in Section 2.2) and an experiment with a realistic SST. All simulations use the same physic, meaning they have the same cloud scheme and subgrid turbulence parametrizations and they also use the same discretization (CEN4TH,RK4,PPM01) of the equations of conservation. The numerical schemes and parametrizations used here are the same as in Jacquet et al. (2025). All simulations use the same vertical levels, ranging from $\Delta_z = 2$ m at the

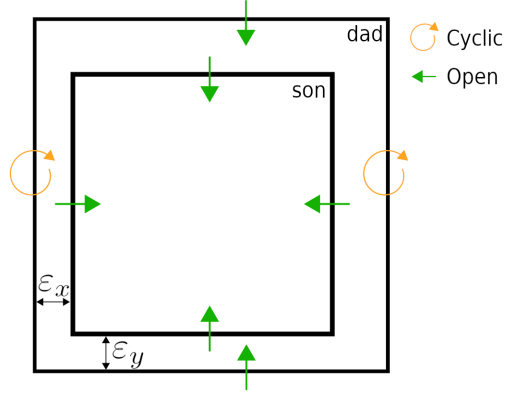


Figure 1. Nesting configuration. Arrows are the boundary conditions for each domains.

surface to $\Delta z = 20$ m at $Z = 2000$ m, the model top. Horizontal grid spacing is uniform and it is the same in X and Y directions. The horizontal resolution Δ_x is 200 m for the dad domains, and 50 m for son domains as well as any homogeneous cyclic configurations. Characteristics specific to each simulations can been found in the Table 1. When using the fourth order central finite difference scheme and fourth order Runge-Kutta for spatial and temporal discretizations for wind advection, a diffusion operator is applied on wind variables to reduce spurious motions. This characteristic time is XT4DIFU and it has to be tuned by the user according to the resolution of the experiment. In our case, a usual value of XT4DIFU = 100 s is used for domains at 50 m resolution, which damp $2\Delta_x$ waves by e^{-1} in 10 timesteps. A value of XT4DIFU = 800 s for the domains at 200 m was found to improve the turbulent inflow for the son domains, compared to a dad domain with a stronger diffusion. The son domain is defined after a period of spinup from the dad domain. The spinup time is one hour for the validation experiment and ??? for the experiment with the realistic SST. Then, the grid of the son domain is defined by ε_x and ε_y which are the number of cells way from the eastern and southern boundaries respectively (in number of cell from the dad domain). We choose to set ε_y in a way that put the the son domain as far as possible to the open boundary condition from the dad domain. ε_x is set to be close the the boundary as the dad East boundary condition is cyclic and thus we do not expect any problem with this type of boundary.

Table 1. Configuration of the simulations

Name	Δ_x (m)	Δ_t (s)	XT4DIFU (s)	N_x	N_y	ε_x	ε_y	SST
Validation								
VALdad	200	4	800	64	64	0	0	N/S gradient or 298 K
VALson	50	1	100	200	200	4	4	N/S gradient or 298 K
RefVal	50	1	100	200	200	4	4	298 K
Experiment								
AGGdad	200	4	800	TBD	TBD	0	0	analysis
AGGson	50	1	100	TBD	TBD	TBD	TBD	analysis
RefC	50	1	100	200	200	-	-	TBD
RefW	50	1	100	200	200	-	-	TBD

2.2 Turbulent inflow validation

This section aims to validate the nesting configuration of Figure 1 as a way to get a turbulent inflow for a LES simulation over an heterogeneity. At first, a nested setup is designed with homogeneous SST of 298 K, giving a fairly convective atmosphere ($z_i/L = ?$). The characteristics of the dad (VALdad) and son (VALson) domains can be found in Table 1. For comparison, a simulation with homogeneous SST (298 K) and cyclic conditions has been run (RefVal in Table 1). Initial conditions are the same for the two simulations: a constant, zonal-only geostrophic wind of 7.5 m.s^{-1} , an idealized boundary layer with constant potential temperature $\theta = 295 \text{ K}$ and moisture mixing ratio $r_v = 10 \text{ g.kg}^{-1}$ under z_i and then a gradient of temperature (3 K.km^{-1}) and moisture ($-4.6 \text{ g.kg}^{-1}.\text{km}^{-1}$). After two hours of simulated time, Figure 2 shows vertical wind. The homogeneous simulation show convective plumes of $?$ the size of the domain. The son domain from the nested configuration has a smooth turbulent inflow coming at turbulent scale of the dad domain. The fetch needed for the turbulence to become ‘at scale’ (in the sens of Nagel et al. (2022)) can be qualitatively seen by spotting the distance where the turbulent structure are not as smooth as the inflow. In this case, we estimate the fetch at around 6 km away from the inflow border, in the zonal direction. We note however that structures from the VALson simulation cover more area than the RefVal case. To validate the fetch quantitatively, we show on Figure 3 cross-wind spectra at several X position (the dominant wind is zonal) and we compare them with the spectrum at the East border of VALson and also cross-wind spectra from RefVal. Spectra show that i) turbulence near the East border of VALson is comparable to the spectra from the homogeneous simulation, meaning that the turbulent scales are now similar to a non-nested configuration ii) the turbulent fech from the West border of VALson is around 4 km, 2 km earlier from the qualitative value. The second point means that the fetch can be first detected ‘by eye’ during a design phase of the setup, and then confirmed with spectra later. This fetch is far less than what was found in a similar configuration but with an open inflow boundary condition that required more than 20 km for turbulence to develop from the inflow condition (a prescribed profile with no perturbation).

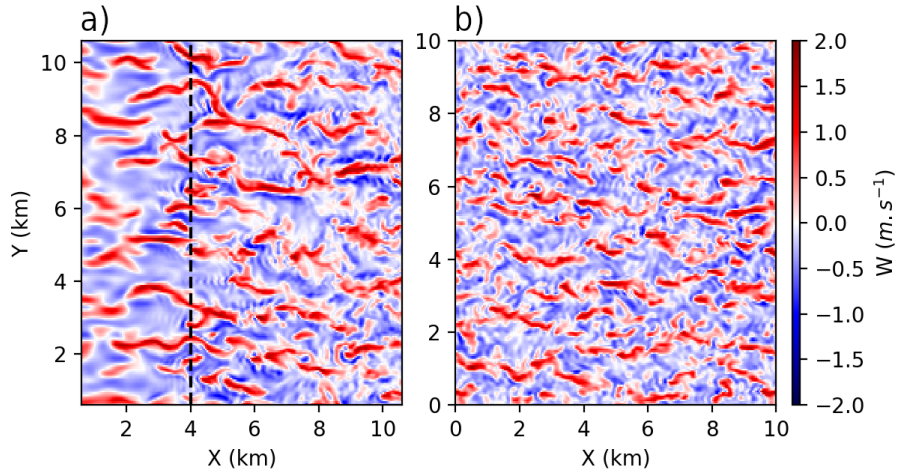


Figure 2. Vertical velocity at $Z = 200 \text{ m}$ for the simulations a) VALson with homogeneous SST and b) RefVal. The vertical dashed line on a) discriminate turbulent scale from dad (left of the line) and son (right of the line) domains.

Having compared turbulent scales, we now compare on Figure 4 profiles of mean quantities for VALson and RefVal. The average operator in the RefVal simulation is an

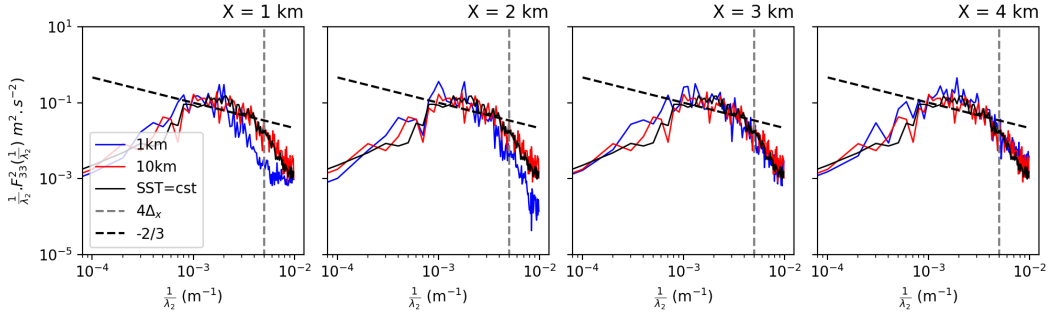


Figure 3. Cross-wind spectra of vertical velocity at $Z = 200$ m, at several X position (in blue) for VALson, at $X = 10$ km (West side of the domain, in red) and for the homogeneous simulation (in black). The grey vertical dashed line is the expected effective resolution of $4\Delta_x$, the black dashed line is the inertial range. Both axis are in log scale.

horizontal average over the whole domain, while the for the VALson simulation the average is an horizontal average over the part of the domain where turbulence is ‘at scale’, i.e. from $X = 6$ km to the East border. Flux are the sum of resolved and subgrid fluxes. Overall, first order statistics profiles are very similar, with a zonal velocity (Figure 4a) from VALson slower by 5 cm.s^{-1} and a better mixed moisture mixing ratio (Figure 4c) in the nested configuration. Turbulent statistics show some discrepancy: $\langle uw \rangle$ profiles from VALson might not be converged, as the average operator has around half the number of points compared to RefVal, buoyancy profiles show good agreement, total turbulent kinetic energy levels from VALson near surface (in the upper ABL) are on par with (higher than) RefVal values.

We find that the nesting configuration with homogeneous SST and the cyclic configuration gives comparable results and so we will use the nesting method to generate a turbulent inflow over a realistic SST gradient.

NOTE Hugo 8/10/24 : pour le cas réel, j'ai utilisé XT4DIFU = 800s pour le domaine père, alors que dans mes tests j'ai utilisé la valeur de 1800s. Peut-être qu'il faudrait mettre à jour le cas test pour que ça colle avec la valeur de XT4DIFU que je vais utiliser dans la simulation réelle finale !

3 The Aghulas current

We now focus on describing the case study of the ‘Experiment’ simulations (Table 1). A brief description of the environmental conditions is given, including an overview of the ERA5 dataset profiles.

Here description of visible, SST L4 reanalysis, SAR vignette, ERA5 profiles/conditions

Here small section about the characteristics of the LES with the realistic SST: 64*90km, dx=50m, size of dad is 108.

4 Methods

For the comparison between SAR and LES images, some ideas were laid out in https://docs.google.com/document/d/1txJJcf0MK0iLx3VaDkNWp8ZrWu_z8LQwvXLLe-V5lys/edit?usp=sharing

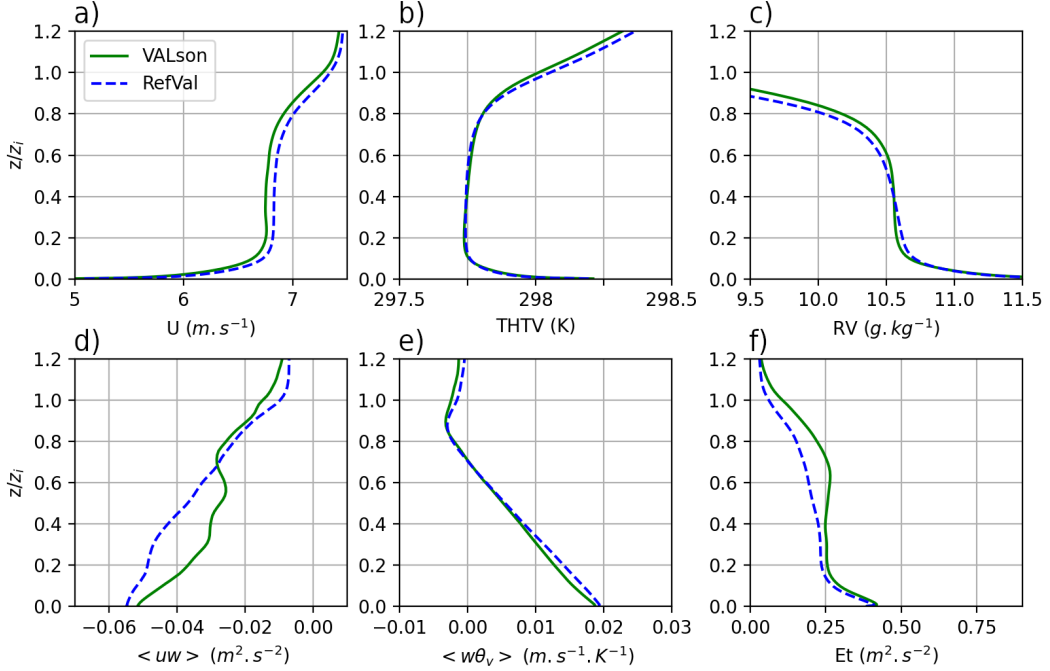


Figure 4. Mean profiles of a) Zonal wind U ($m.s^{-1}$), b) virtual potential temperature θ_v (K), c) moisture mixing ratio r_v ($g.kg^{-1}$) d) total vertical flux of zonal momentum $\langle uw \rangle$ ($m^2.s^{-2}$), e) buoyancy flux $\langle w\theta_v \rangle$ ($m.s^{-1}.K^{-1}$) and f) total turbulent kinetic energy Et ($m^2.s^{-2}$). See the text for the definition of the average operators.

4.1 Conditional sampling based on passive tracer

Short description of the conditional sampling, link to 1rst paper

4.2 Spatial statistics

4.2.1 Structure function

Structure function (Granero Belinchon et al., 2022) has been used to find characteristic length scale for roll organization of the ABL (Brilouet et al., 2023). They are defined, in polar coordinate and at the order N, for a 2D field F, by:

$$S_N^{r_\theta, r_\rho} = \langle (F(r + r_\rho, \theta + r_\theta) - F(r, \theta))^N \rangle \quad (1)$$

where r and θ are spatial positions, r_θ and r_ρ are spatial lags and $\langle . \rangle$ is the average operator (X and Y average in our case). This structure function is computed with *Nth_structure_function_2D* and it uses Dask to compute in parallel $S_N^{r_\theta, r_\rho}$ for each values of r_θ and r_ρ . On top of this, we fit an ellipse following Brilouet et al. (2023) to get characteristic length scale for the case where a roll organization is dominant. This needs to be tweaked: I still have not test case to verify that my implementation is working as intended, and also in our case there is not much roll case.

4.2.2 Monin-Obukhov length estimate

How L is estimated for SAR data (O'Driscoll et al., 2023), how we compute it in LES simulation (ref Stull).

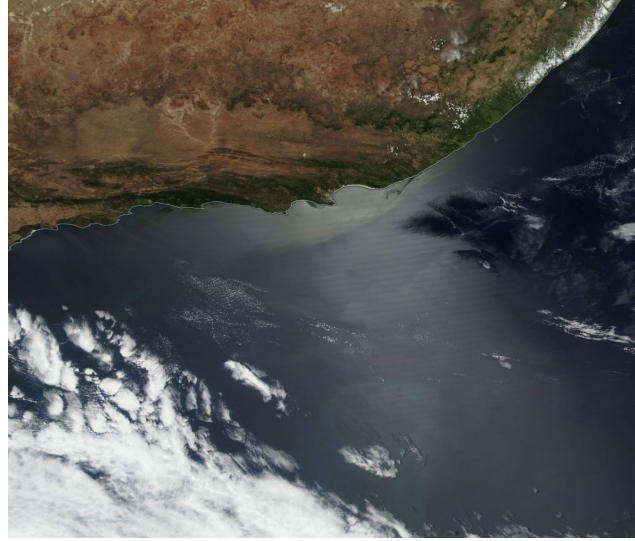


Figure 5. Suomi NPP visible 10th dec 2015, aerosols are present. Bounds are -39°N/-32°N, 20°E/30°E.

4.2.3 Coherent structure characteristic size

The coherent structures are detected with the C10 method. We can now look for a characteristic size of the objects. We do this by searching for an equivalent radius for each structure with the function `R_equivalent_for_all_objects`. For each structure s (e.g. updraft), we use `scipy.ndimage.label` to label each aggregate of the structure in the plan XY. Then for each label, we take the equivalent radius as:

$$R_{eq}(s, i, z) = \left(\frac{1}{\pi} \cdot N_i \Delta_x \Delta_y \right)^{1/2} \quad (2)$$

with N_i the number of cell of label i at the altitude z of the object s . We then look at the distribution of this equivalent radius at each altitude. We plot the most represented mode (in grey) and the averaged equivalent radius (in white) on Figure 8. The mean equivalent radius is also plotted on Figure 9 for comparison between objects.

4.3 Environment influence

Here description of the environmental conditions that will be investigated. To be changed : geo wind speed, height of initial boundary layer, intensity of inversion, temperature/moisture of initial boundary layer (mixed layer part).

Case 1 is ERA5, other cases needs to be defined.

5 Results

5.1 Lagrangian wind budget

The first step in the simulation analysis is to study the wind budget. I suggest to use a Lagrangian wind budget, much like in Redelsperger et al. (2019).

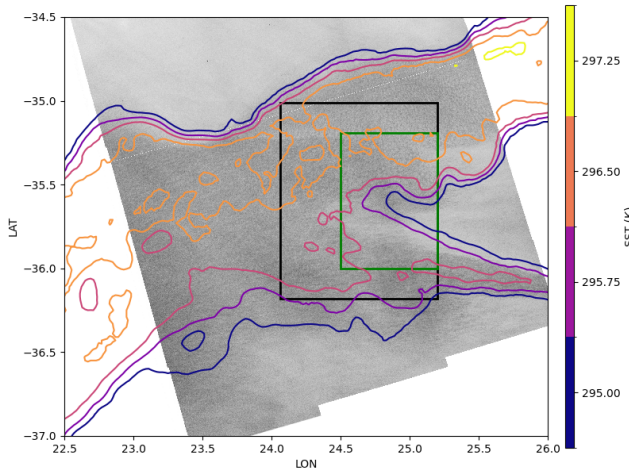


Figure 6. Normalized SAR roughness from Sentinel-1A, swath of the 10th of December 2015, 17h08 UTC, south of South Africa (10-12-2015 absolut orbit number 8982, numéro de vignette, product unique ID) and contours of SST from L4 Regional product from Ifremer. Rectangle are the LES domains (work in progress).

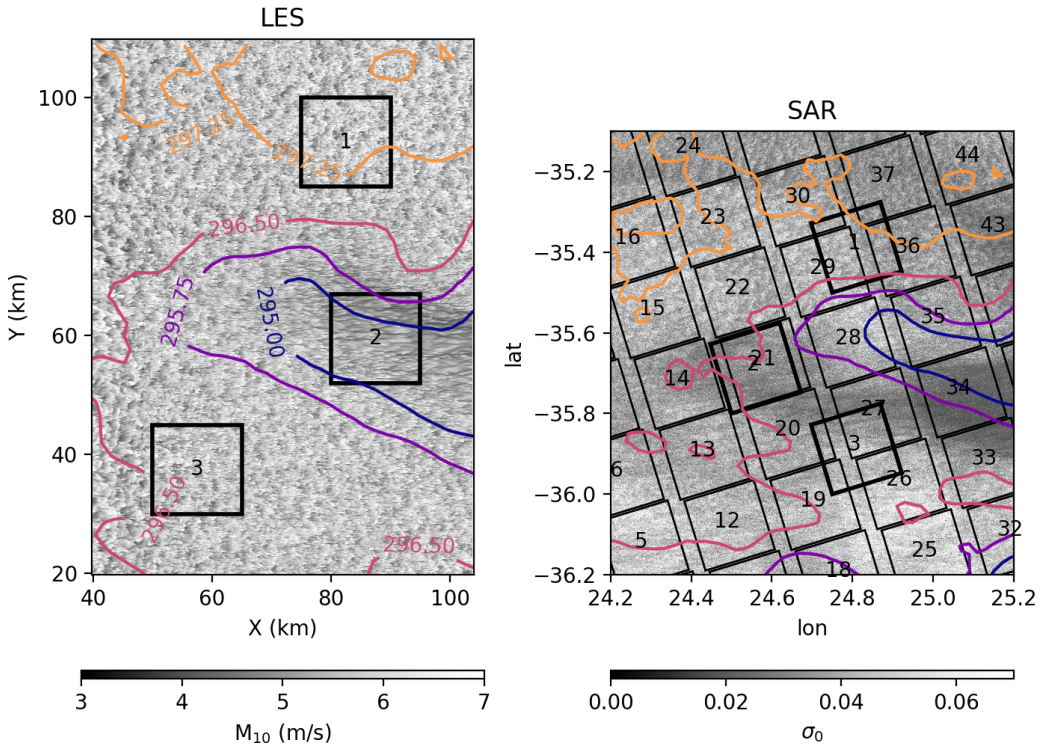


Figure 7. Boxes location for SAR et LES (child domain) data. The choice of position of boxes can be automated for the SAR (it is the background of tiles numbered ≥ 4 on the present image) but user can still specify location of interest (tiles 1 to 3 here). Background is the modulus of the 10 m wind for the LES, and the detrend surface roughness for the SAR. Contours are the SST analysis ODYSSEA.

5.2 Coherent structure leaves imprints on the surface roughness

Here I suggest to describe a figure with in the background a surface field (10 m wind field for example), and above this in contours the coherent structure at some altitude Z. The goal is to find visual similarities between the surface and what happens above.

5.3 Characteristic length scale in LES and SAR data

Using length scale retrieved from different methods (structure functions, equivalent radius or the MO length estimate), can we find a common value for LES and SAR? And at what altitude in the LES?

This paragraph describes Figure 8 and 9. We see on Figure 9 that in boxe 1 and 3, the objects updraft 1 and subsiding shells 1 are not present. In all boxes, the down-drafts see a drop in R_{eq} at z_i or slightly above. This is because the tracer 3 is emitted the same at every altitude using a domain averaged virtual potential temperature to compute a ABL height. It is then emitted 50 m above this height. This could be improve by modifying the code to take into account local variability of z_i . In Figure 8, we can see that at a specific Z and for every objects, the most represented mode (solid grey line) has a lower R_{eq} than the average equivalent radius (solid white line). Typical R_{eq} for up1 is greater than for up2, which is expected as boxe 2 is over a zone where only tracer 1 is emitted. Subsiding shells (ss1 and ss2) share similar values of R_{eq} . No downdraft are detected below the ABL height.

5.4 Linking surface roughness to vertical structure

For the length scale identified in the previous section, how can we infer the structure of the ABL from the surface field with the use of coherent structure ? Let's try to give the atmosphere structure (i.e. flux decomposition) above the SAR vignettes.

6 Discussion

7 Conclusion

Open Research Section

SAR data from Sentinel-1A are made available by the European Copernicus program at WEBSITE. The numerical code used to produce the simulations is MesoNH (version 5.7.0, <http://mesonh.aero.obs-mip.fr/mesonh57/Download>), namelists and post-process scripts are available on the GitHub repository (https://github.com/HugoJacq/Linking_SAR_and_ABL_structure).

Acknowledgments

References

- Brilouet, P.-E., Bouniol, D., Couvreux, F., Ayet, A., Granero-Belinchon, C., Lothon, M., & Mouche, A. (2023, January). Trade Wind Boundary Layer Turbulence and Shallow Precipitating Convection: New Insights Combining SAR Images, Satellite Brightness Temperature, and Airborne In Situ Measurements. *Geophysical Research Letters*, 50(2), e2022GL102180. doi: 10.1029/2022GL102180
- Couvreux, F., Hourdin, F., & Rio, C. (2010). Resolved versus parametrized boundary-layer plumes. Part I: a parametrization-oriented conditional sampling in Large-Eddy Simulations. *Boundary-Layer Meteorology*, 134(3), 441–458. doi: 10.1007/s10546-009-9456-5

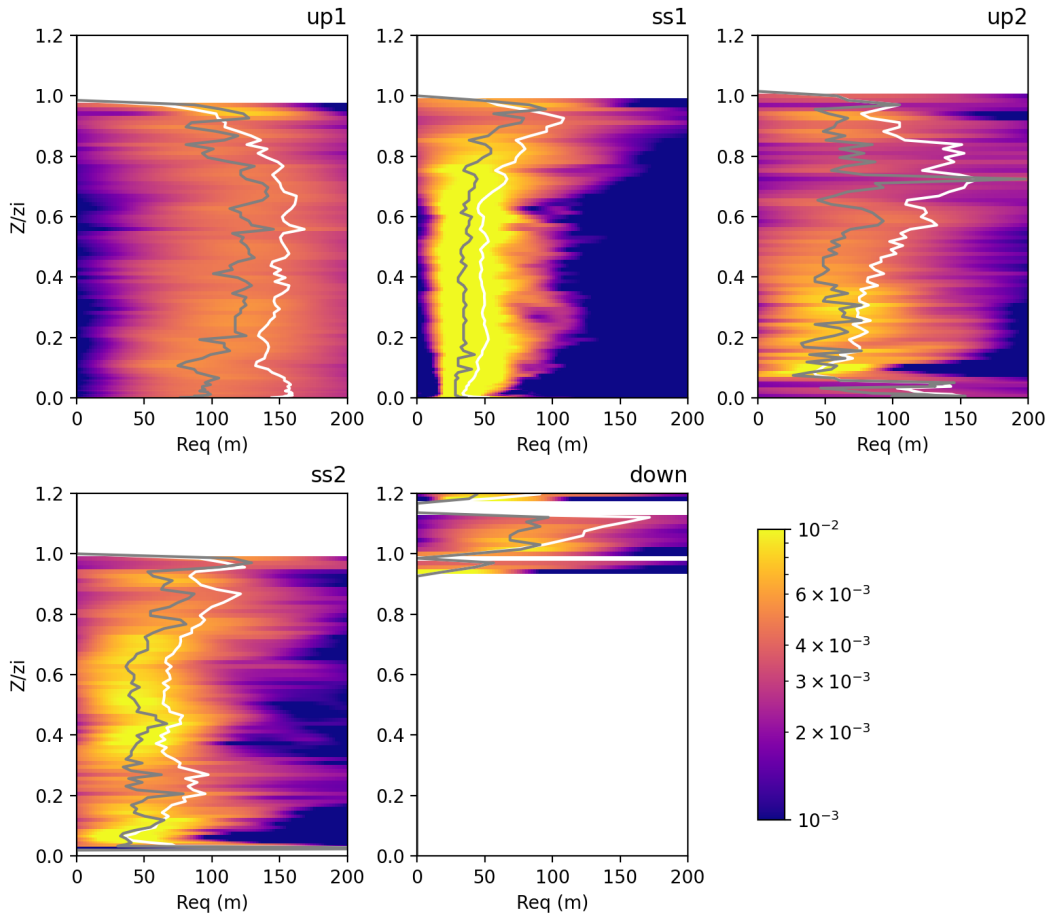


Figure 8. LES data. PDF of equivalent radius for boxe 2 at each altitude and for each objects. Solid grey profile is the most represented mode, solid white is the averaged radius. A white background means that the object has not been detected (see Figure 9).

- Fogarty, J., Bou-Zeid, E., Bushuk, M., & Boisvert, L. (2024, September). How many parameters are needed to represent polar sea ice surface patterns and heterogeneity? *The Cryosphere*, 18(9), 4335–4354. doi: 10.5194/tc-18-4335-2024
- Granero Belinchon, C., Roux, S. G., Garnier, N. B., Tandeo, P., Chapron, B., & Mouche, A. (2022, September). Two-dimensional structure functions for characterizing convective rolls in the marine atmospheric boundary layer from Sentinel-1 SAR images. *Remote Sensing Letters*, 13(9), 946–957. doi: 10.1080/2150704X.2022.2112107
- Jacquet, H., Ayet, A., & Couvreux, F. (2025). Atmosphere Response to an Oceanic Sub-mesoscale SST Front: A Coherent Structure Analysis [preprint]. *Journal of Geophysical Research: Atmospheres*. doi: <https://hal.science/hal-04729066>
- Lac, C., Chaboureau, J.-P., Masson, V., Pinty, J.-P., Tulet, P., Escobar, J., ... Wautelet, P. (2018). Overview of the Meso-NH model version 5.4 and its applications. *Geoscientific Model Development*, 11(5), 1929–1969. doi: 10.5194/gmd-11-1929-2018
- Nagel, T., Schoetter, R., Masson, V., Lac, C., & Carissimo, B. (2022, July). Numerical Analysis of the Atmospheric Boundary-Layer Turbulence Influence on Microscale Transport of Pollutant in an Idealized Urban Environment. *Boundary-Layer Meteorology*, 184(1), 113–141. doi: 10.1007/s10546-022-00697-7

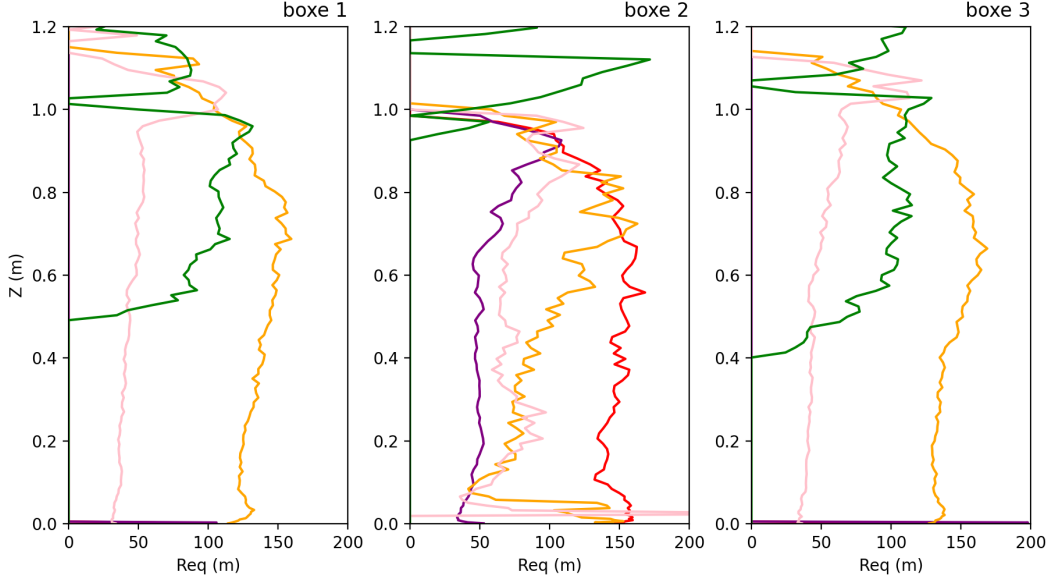


Figure 9. Equivalent radius for each object in the LES, averaged over the XY plan for each boxe, at all altitude. Object color is: red for updraft 1, purple for subsiding shell 1, orange for updraft 2, pink for subsiding shell 2 and green for downdrafts.

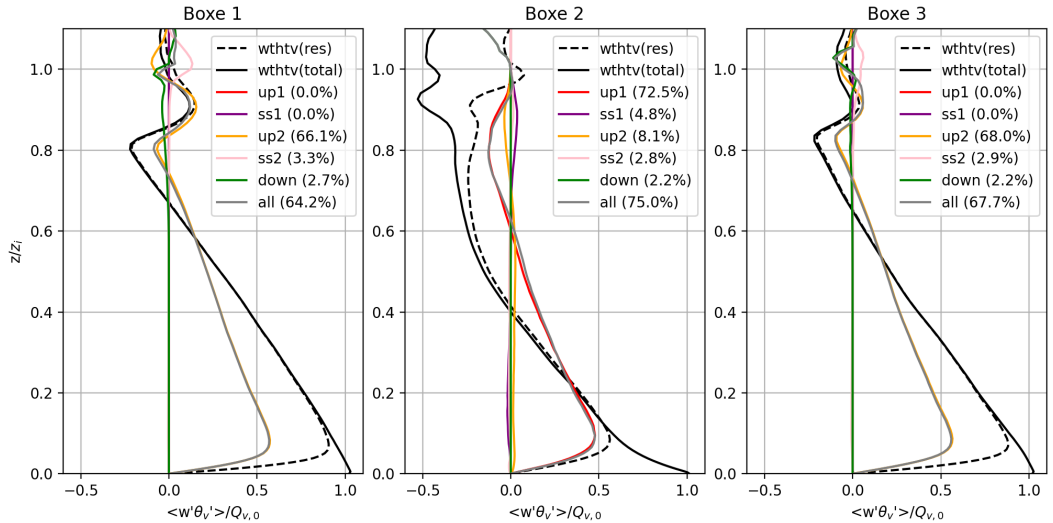


Figure 10. LES buoyancy flux profile, for each boxes. The flux is decomposed into contributions from coherent structures. Tracer 1: ‘up’ is updrafts and ‘ss’ is subsiding shells. Tracer 2: ‘up2’ is updrafts and ‘ss2’ is subsiding shells. Tracer 3: ‘down’ is downdrafts. Grey solid line is the contribution from all structure. The percentage in the legend is the vertically integrated contribution.

O'Driscoll, O., Mouche, A., Chapron, B., Kleinherenbrink, M., & López-Dekker, P. (2023, August). Obukhov Length Estimation From Spaceborne Radars. *Geophysical Research Letters*, 50(15), e2023GL104228. doi: 10.1029/2023GL104228
 Redelsperger, J.-L., Bouin, M.-N., Pianezze, J., Garnier, V., & Marié, L. (2019). Impact of a sharp, small-scale SST front on the marine atmospheric bound-

ary layer on the Iroise Sea: Analysis from a hectometric simulation. *Quarterly Journal of the Royal Meteorological Society*, 145(725), 3692–3714. doi: 10.1002/qj.3650